Check for updates

Influence of counterion type on the scattering of a semiflexible polyelectrolyte†

Anish Gulati, [ID] [a] Jack F. Douglas, [ID] [b] Olga Matsarskaia [ID] [c] and
Carlos G. Lopez [ID] *[ad]

Understanding the influence of counterion and backbone solvation on the conformational and thermodynamic properties of polyelectrolytes in solution is one of the main open challenges in polyelectrolyte science. To address this problem, we study the scattering from semidilute solutions of a semiflexible polyelectrolyte, carboxymethyl cellulose (CMC) with alkaline and tetra-alkyl-ammonium (TAA) counterions in aqueous media using small-angle neutron scattering (SANS), and small-angle X-ray scattering (SAXS), which allow us to probe concentration fluctuations of the polymer backbone and counterions. In SAXS, the calculated contrast arises primarily from the polymer backbone for both alkaline and TAA salts of CMC. In SANS, however, the contrast is dominated by the counterions for the TAA salts and the polymer backbone for the alkaline salts. Solutions are found to display a correlation peak in their scattering function, which at low concentrations is independent of counterion type. At moderate salt concentrations ($c \gtrsim 0.1$ M), the peak positions obtained from SANS and SAXS for the CMC salts with the TAA counterions differ. This divergence suggests a decoupling in the lengthscale over which the couterions and the polymer fluctuate. Upturns in the scattering intensity in the low-q region signal the presence of long-ranged compositional inhomogeneities in the solutions. The strength of these decreases with increasing counterion–solvent interaction strength, as measured by the viscosity B coefficient, and are strongest for the corresponding sodium salt of CMC.

I. Introduction

Polyelectrolytes are polymers with charged groups covalently bonded to their backbone. The presence of these charges lends them an array of properties leading to a significantly different behaviour compared to their neutral counterparts.[1–3] These properties can be further modified by altering the interaction between the charges by, for instance, the addition of low molecular weight salts, or by varying the counterion type.[3–14] The importance of biological polyelectrolytes such as DNA, RNA, hyaluronic acid or proteoglycans makes understanding the physics of charged polymers crucial for understanding fundamental biological phenomena and molecular interactions.[15,16]

[a] Institute of Physical Chemistry, RWTH Aachen University, Landoltweg 2, 52056 Aachen, Germany

[b] Materials Science and Engineering Division, National Institute of Standards and Technology, Gaithersburg, Maryland 20899, USA

[c] Institut Laue-Langevin DS/LSS, 71 avenue des Martyrs, CS 20156, 38042 Grenoble Cedex 9, France

[d] Department of Material Science and Engineering, The Pennsylvania State University, University Park, Pennsylvania 16802, USA. E-mail: cvg5719@psu.edu

† Electronic supplementary information (ESI) available. See DOI: **https://doi.org/10.1039/d4sm00874j**

The role of counterion solvation, which was usually not considered in early polyelectrolyte solution theories,[17–22] has received increasing attention in recent years[5,23–27] and this phenomenon is thought to be responsible for some hitherto unexplained phenomena in polyelectrolyte solutions, such as the low-q upturn observed in the structure factor of solutions of low ionic strength. Several recent simulation studies discuss the effect of counterion solvation on the properties of polyelectrolyte solutions. For example, it is known that the relative quality of the solvent for the polymer backbone and counterions can influence the distribution of counterions around the chain.[28] Using a coarse-grained model of polyelectrolyte solutions with explicit solvents, Chremos and Douglas concluded that with increasing affinity of the counterions to the solvent, the solution becomes increasingly heterogeneous due to supramolecular chain association.[23,29] This phenomenon naturally gives rise to a stronger upturn in the scattering intensity at low-q, a phenomenon ubiquitously observed in synthetic polyelectrolytes, as well as proteins, and many other biomolecule solutions.[23] This finding was further backed by another molecular dynamics simulation study that investigated the effect of altering the relative solvation of the counterions and the backbone. The latter study indicated a stronger upturn at low-q for a preferential solvation of the counterion.[25] Another molecular dynamics (MD) simulation study

found that the stronger solvation of the charged species (counterion and backbone alike) leads to the disappearance of the correlation peak and a strong low-q upturn,[24] a behaviour observed in aggrecan[30] and other highly charged bottlebrush polyelectrolyte molecules in which the sidegroups are highly hydrophilic. This result was interpreted as arising from the appearance of short and long-ranged attractive forces induced by the better-solvated counterions, which leads to the formation of heterogeneous multichain structures. The work of Wang et al.[31] provides additional evidence for the importance of solvent-specific effects[32] on the electrostatic interactions between charged objects in solution, that are not captured by continuum electrostatics. According to their model, polar solvents can order around charged objects in a way that strongly depends on the sign of the charge on the object, suggesting another level of subtlety in the interactions between charged particles and polymers in solution.

The existence and behaviour of the multichain domains in polyelectrolyte solutions have been studied in the literature, primarily using dynamic light scattering (DLS).[3,5,33–40] These domains have been recognised as the source of the slow mode on the DLS correlation curves, and the low-q upturn in small-angle neutron scattering (SANS)/small-angle X-ray scattering (SAXS) curves[38,41,42] and have been found to exist for a range of systems. Their response to different stimuli, such as ionic strength[34] and mechanical filtration,[36,39] and their stability over time[37] have been reported. These domains have been found to be stable for long periods of time under no-added salt conditions for systems such as sodium polystyrene sulfonate, and ionised solutions of polyacrylic acid and polymethacrylic acid.[37] Filtering has been shown to transiently alter their properties and non-equilibrium effects have sometimes been observed.[36,39]

In the present work, we study the scattering of carboxymethyl cellulose aqueous solutions as a function of counterion type. Carboxymethyl cellulose (CMC), usually employed as its sodium salt NaCMC, is a weak, semiflexible polyelectrolyte which is widely employed as a rheology and texture modifier in food, drinks, pharmaceutical products and in drilling muds.[43–46] With a market size of over USD 1 billion,[47] it is the most widely employed cellulose ether as well as the most important ionic derivative of cellulose.[48]

The monomer structure of CMC is shown in Fig. 1. R = H in all three positions corresponds to cellulose. The degree of substitution (DS) is the average number of R = CH$_2$COO$^-$X$^+$ groups per monomer, out of a maximum of 3. The structural and rheological properties of NaCMC have been extensively studied in earlier publications.[49–59] Grades with DS $\gtrsim$ 1 are labelled as "highly substituted" and usually display "hydrophilic" behaviour in aqueous solution,[52,54] meaning that inter-chain associations are relatively weak and no crystalline aggregates of unsubstituted cellulose are present.[50,51,60–63] In aqueous solution, NaCMC displays a locally rigid conformation,[50,51,64] independent of degree of substitution. Its rheological properties in excess salt show similar features to those of other semiflexible polysaccharides (neutral or charged).[43,65,66] Despite extensive investigations into the properties of CMC, literature on the influence of counterion on the solution behaviour of CMC are limited to a few studies on their electrical conductivity.[67,68]
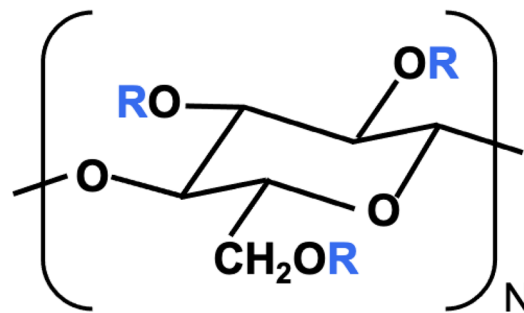

Fig. 1 Carboxymethyl cellulose monomer where R = H or CH$_2$COO$^-$X$^+$ and X$^+$ is the counterion. The degree of substitution (DS) is the number of R = CH$_2$COO$^-$X$^+$ per monomer, out of a maximum of three.

II. Background theory

The relatively expanded nature of polyelectrolytes in salt-free solutions, compared to their uncharged counterparts, means that the overlap concentration[2,52] is very low, and semidilute or concentrated solutions are usually of interest. The scaling theory of Dobrynin et al.[17] models semidilute polyelectrolyte solutions based on the assumption of well-dispersed chains with a characteristic mesh size known as the correlation length ξ, which, in the absence of added salts, is predicted to scale with polymer concentration (c) as,

$$\xi = \left(\frac{B_s}{bc}\right)^{1/2} \tag{1}$$

where b is the monomer length and B_s is a stretching parameter which quantifies the degree of folding of the polyelectrolyte chain inside a correlation blob. A value of $B_s = 1$ corresponds to fully stretched chains and $B_s > 1$ indicates local folding. While this is an idealized model that does not address the long-range attraction effects that can arise from ion solvation, this model nonetheless captures many observed trends in polyelectrolyte solutions, and we refer to the predictions of this reference model in our discussion below.

For example, the predicted variation of $\xi \propto c^{-1/2}$ from this model is consistent with reports on many experimental studies on flexible,[2,69–72] semiflexible[50,51,64,73] and rigid polyelectrolyte systems.[74] In this scaling model, the correlation length (ξ) characterizes the lengthscale at which polyelectrolyte chains become flexible, in agreement with experimental observations for polystyrene sulfonate.[75]

Although a scaling exponent having a magnitude near 1/2 is common, this exponent is not universal. Values of this scaling exponent near 1/3 have been observed in mucin bottlebrush polyelectrolytes[76] and proteoglycan molecules from cartilage[77] where strongly hydrating side-groups exist, as in the case of aggrecan. This exponent also matches the observation of Kaji et al. for polyelectrolytes in dilute solutions.[78,79] Chremos and Douglas[29] found by simulation with an explicit solvent that the magnitude of this scaling exponent can be reduced from 1/2 when the counterions or polymer are strongly hydrating and a smaller magnitude exponent has been observed in poly-ionene solutions with certain counterions.[80] Simulation and measurement also indicated an exponent having a value near

1/3 in star polymer polyelectrolytes[81,82] and an exponent value near 1/3 has been observed in dendrimer polyelectrolytes,[83,84] globular proteins[85,86] and other relatively compact-shaped charged polymers and charged particles such as charged micelles.[87,88] Changes in the value of the polyelectrolyte peak scaling exponent might then provide a clue about new physics in these solutions becoming important. We will see this situation arise below in our discussion of tetraalkylammonium counterions of carboxymethyl cellulose.

A. Partial structure factors and scattering contrast

SANS. Following the notation of van der Maarel et al.,[89] the neutron scattering of a polyelectrolyte solution, in the absence of added salts can be written as,

$$I(q) = \rho_m \overline{b}_m^2 S_{mm}(q) + 2\sqrt{\rho_m \rho_c}(\overline{b}_m \overline{b}_c) S_{mc}(q) + \rho_c \overline{b}_c^2 S_{cc}(q) \tag{2}$$

where $S(q)_{m,m}$, $S(q)_{m,c}$ and $S(q)_{c,c}$ are the partial structure factors, for monomer–monomer, monomer–counterion and counterion–counterion correlations respectively and ρ_m and ρ_c are the concentrations in number per unit volume for the monomer and the counterion respectively. If x is the degree of substitution, $\rho_c = x \times \rho_m$, and therefore we have,

$$\frac{I(q)}{\rho_m} = \overline{b}_m^2 S_{mm}(q) + 2\sqrt{x}(\overline{b}_m \overline{b}_c) S_{mc}(q) + x\overline{b}_c^2 S_{cc}(q) \tag{3}$$

The contrast factors for SANS are given by,

$$\overline{b}_i = b_i - b_s \frac{v_i}{v_s} \tag{4}$$

where b_i and v_i are the scattering length and volume of the unit. The subscript s refers to the solvent and i = c or i = m.

If the concentration fluctuations of counterions and the polymer backbone occur on the same lengthscale, which is expected, for example, if a large fraction of the counterions are condensed onto the backbone, we can simplify eqn (2) using the approximation $S_{m,m}(q) \simeq S_{m,c}(q) \simeq S_{c,c}(q)$. The structure factor can then be calculated from the scattering intensity as:

$$S(q) \simeq (\overline{b}_{eff})^{-1} \frac{I(q)}{\rho_m} \tag{5}$$

where we define the effective contrast factor as:

$$\overline{b}_{eff} = \overline{b_m}^2 + 2\sqrt{x}(\overline{b_m b_c}) + x\overline{b_c}^2 \tag{6}$$

note that $\overline{b}_{eff}$ has units of length squared.

B. Scattering functions for semidilute polyelectrolyte solutions

The total structure factor $S(q)$ can be written as the sum of an interparticle contribution, known as the form factor ($P(q)$) and an intermolecular term $H(q)$:

$$S_{m,m}(q) = NP(q) + \rho H(q) \tag{7}$$

For sufficiently high wave-vectors,[89,90] $H(q) \simeq 0$, and we approximate $S_{m,m} \approx NP(q)$. Chains are expected to be in a rigid configuration inside the correlation blob, so that for $q \gg 2\pi/\xi$,

$P(q)$ may be approximated by the form factor of a rod:[89]

$$I(q) \simeq \rho_m \overline{b}_{eff} \left[\frac{\pi}{b'q} \right] e^{-q^2 R_C^2/2} + I_{Bck} \tag{8}$$

where R_C is the cross-sectional radius of the chain, b' is the z-projected monomer length and c the concentration in number of monomers per unit volume.[91] The term in square brackets corresponds to the form factor of an infinitely thin-rod and the exponential takes into account the finite lateral dimensions of the chain. The constant I_{Bck}, which is left as a free parameter accounts for the q-independent scattering. This includes contributions from incoherent scattering (spin incoherence), arising primarily from ^1H isotopes as well as coherent q-independent contributions (known as compositional incoherent or Laue scattering).

Polyelectrolytes, normally, display a peak in their scattering function at wave-vector q^*, which defines a correlation length as:[17,19]

$$\xi = \frac{2\pi}{q^*} \tag{9}$$

Experimentally, a large upturn in the scattering intensity is also normally observed at low scattering wave-vectors (q), the origin of which remains controversial because the very low osmotic compressibility of salt-free polyelectrolyte solutions might be expected to strongly suppress concentration fluctuations over long length-scales. The origin of the upturn has been assigned to multichain clusters of polyelectrolyte chains, undissolved aggregates, or long-ranged concentration fluctuations, as discussed in the introduction.[23,38] Simulations that have not included a description of solvation have not observed this phenomenon so the solvation seems to be qualitatively implicated.

For wave-vectors $R_{g,C} \lesssim q \ll 2\pi/q^*$, where $R_{g,C}$ is the radius of gyration of the clusters, the scattering intensity can be described by a power-law:

$$I(q) = Dq^{-m} \tag{10}$$

where m is the apparent fractal dimension of the clusters, which can take values between 1 (rod-like clusters) and 3 (compact clusters). Exponents larger than 3 are characteristic of surface fractals and compact objects with sharp interfaces.[92,93] Experimentally, m has been observed to vary between -4.3 to -2.1.[38,50,51,94,95]

For sufficiently small wave-vectors $q \lesssim 1/R_{g,C}$, the Guinier law describes the scattering intensity:

$$I(q) = I(0)e^{-q^2 R_{g,C}^2/3}$$

where $I(0)$ is proportional to the contrast between the polyelectrolyte and solvent and the concentration of clusters and their molar mass. Most static scattering experiments, with few exceptions[34,92] do not cover a sufficiently broad q-range to make an accurate determination of the cluster size possible. Dynamic light scattering experiments yield apparent hydrodynamic sizes of the clusters in the range of a few hundred nanometers.[92,96,97]

III. Materials and methods

Materials

NaCMC was purchased from Sigma-Aldrich, with a nominal mass average molar mass (M_w) of 250 kg mol^{-1} and degree of substitution (DS) = 1.2. Characterisation of the sample in an earlier study[96] yielded $M_w \simeq 2.1 \times 10^5$ g mol^{-1} and DS = 1.3. The Spectra/Por dialysis membranes[98] with a Molecular Mass Cut-Off of 6 to 8 kDa were used and were purchased from VWR. A viscosity standard solution N2 purchased from VWR. The bases used for the preparation of CMC salts were acquired from Sigma Aldrich and their characteristics are reported in Table ST2 in the ESI.†

Preparation of CMC salts

As a precursor to the CMC salt preparation, the NaCMC was converted to its acid form (HCMC) by displacement using 0.1 mol L^{-1} HCl at pH $\approx$ 2 and then dialysing the resulting solution against DI water to remove the excess ions. The end point of the dialysis was determined by examining the conductivity of the dialysis bath at the point when the conductivity stayed below 2 µS cm^{-1} beyond, at least, 4 h from the last exchange. The resulting solution was frozen using liquid nitrogen and dried under vacuum at a pressure of 0.4 mbar for 72 h to 96 h.

For the preparation of the CMC salts with alkali metal and quaternary ammonium counterions, the resulting dry HCMC was neutralized with excess of the respective bases. The neutralized solutions were again subjected to the same dialysis and freeze-drying process to obtain the pure salts.

Sample preparation

The CMC salts were stored in the vacuum freeze dryer for $\approx$ 24 h before any samples were prepared. The samples were prepared in polypropylene microcentrifuge tubes, previously washed with deionized (DI) water and dried at 60 °C. All the sample components were added by weight using a weighing balance with a least count of 0.1 mg and, therefore, a typical error of $\pm$0.05 mg.

Densitometry

The density measurements were performed using the Anton Paar DMA 5000 densitometer with a least count of 10^{-6} g cm^{-3}. The accuracy of the instrument was calibrated using DI water.

Thermogravimetric analysis

The PerkinElmer STA 6000 was used for the thermogravimetric measurements to estimate the residual water content in all the CMCs. The sample temperature was increased to 120 °C at 10 °C min^{-1}, and was allowed to reach equilibrium. The temperature was then increased to 550 °C to estimate the point of CMC degradation.

Conductivity and pH

The conductivity measurements were made using the Mettler Toledo S47 SevenMulti conductivity meter. All the pH measurements were made using the Metrohm 744 pH meter at room temperature.

Small-angle neutron scattering

The SANS measurements were carried out at NG30m at NIST Center for Neutron Research (NCNR), Maryland, USA, D11 at Institut Laue-Langevin (ILL), Grenoble, France and SANS-1 at Paul Scherrer Institute (PSI), Switzerland. The sample-to-detector distances (SDD) used at NCNR were 1.5 m and 7 m which covered a q-range of (0.003 to 0.42) Å^{-1} (λ = 6 Å). The measurements at D11 were performed at five different SDDs (1.7 m, 5.5 m, 8 m, 12 m and 28 m) covering a q-range of (0.002 to 0.55) Å^{-1} (λ = 6 Å). The measurements at SANS-1 were conducted at two different SDDs (3 m and 11 m) covering a q-range of (0.005 to 0.36) Å^{-1} (λ = 6 Å). The samples were measured in banjo cells with path lengths of 1 mm, 2 mm or 5 mm depending on polymer concentration.

Small-angle X-ray scattering

The SAXS measurements were carried out at the SPring-8 synchrotron facility, Hyogo, Japan and at the Institute of Physical Chemistry, Rheinisch-Westfälische Technische Hochschule (RWTH) Aachen using an in-house instrument. The sample-to-detector distances of 2 m and 4 m were used at SPring-8, providing a q-range of (0.0023 to 0.2) Å^{-1} using a beam energy of 10 keV. A Peltier heating system was used to maintain the sample temperature at 25 °C. The in-house instrument consists of a 3-pinhole S-Max3000 system with a MicroMax002+ X-ray microfocus generator from Rigaku and a 2D multiwire detector with an active diameter of 200 mm. The sample-to-detector distance of 2.6 m was used, which covered a q-range of (0.005 to 0.4) Å^{-1} (λ = 1.54 Å, Cu radiation). The samples were measured in sealed 1.5 mm (in-house experiments) or 2 mm (synchrotron experiments) borosilicate capillaries from WJM Glas Müller GmbH.

All the measurements were performed at 25 °C, except the conductivity and pH measurements, which were carried out at room temperature ($\approx$ 22 °C). All the data for this study are provided in tabulated form in the ESI.†

IV. Results and discussion

A. Density measurements

The partial molar volume ($\bar{v}$) of various CMC salts were determined from density measurements of solutions using:[99]

$$\bar{v} = \frac{1}{d_s} - \frac{1}{C}\left(\frac{d}{d_s} - 1\right) \quad (11)$$

where d and d_s are the densities of the solution and the solvent (H$_2$O in all cases), and C is the concentration in units of mass of solute per volume of solution. The partial molar volume (PMV) of the CMC monomer without the counterion is estimated as follows: firstly, the PMV of LiCMC was calculated from its solution density. This was used to determine the molar volume of the CMC monomer by subtracting the molar volume of Li$^+$ ion obtained from literature.[100] Assuming that the contribution of the CMC monomer to the partial molar volume of the salt is independent of the counterion, we calculate $\bar{v}$ for the various counterions studied, see Table 1. Values for the PMV of counterions available in literature have also been provided in the table. These are found to be in reasonable agreement with our data except for K$^+$ and Cs$^+$.

Table 1 SANS contrast factor ($\bar{b}_i$) with respect to D$_2$O (SANS) and H$_2$O (SAXS) and partial molar volume for the CMC monomer (DS = 1.3) and the various counterions studied. The values in brackets for the PMV are taken from literature

Scattering unit	b_i SANS [fm]	b_i SAXS [fm]	$\bar{b}_i^2$ SANS [fm^2]	$\bar{b}_i^2$ SAXS [fm^2]	PMV (lit.) [cm^3 mol^{-1}]
CMC$^-$ monomer	54.39	360.39	7680	22 800	133.90
Li$^+$	−1.90	5.64	7.7	18.8	0.83[a]
Na$^+$	3.63	28.2	1.0	591	2.47 (2.68[a])
K$^+$	3.67	50.7	110	893	13.3 (6.63[a])
Cs$^+$	5.42	155	960	10 300	34.3 (12.39[a])
TMA$^+$	−8.91	121	11 030	418	90.6 (84.85[b])
TEA$^+$	−12.24	211	3620	2610	168 (143.53[b])
TBA$^+$	−18.90	392	141 600	18 200	337 (271.18[b])

[a] Ref. 100. [b] Ref. 101.

Table 2 Contrast conditions for alkaline (Li$^+$, Na$^+$, K$^+$ and Cs$^+$) and tetra-alkyl-ammonium (alkyl = methyl, ethyl, butyl) salts

Salts	SANS	SAXS
Alkaline	$I(q) \sim S_{mm}(q)$	$I(q) \sim S_{mm}(q)^a$
TAA	$I(q) \sim S_{cc}(q)$	$I(q) \sim S_{mm}(q)^a$

[a] For CsCMC and TBACMC, the monomer and counterion both contribute siginificantly to $S(q)$.

Table 1 lists the contrast factors for the CMC monomer and the various counterions studied in D$_2$O. Both SANS and SAXS contrast factors for alkali salts in D$_2$O and H$_2$O respectively are dominated by the polymer backbone so that $I(q) \propto S_{m,m}(q)$, with the exception of CsCMC, where the SAXS intensity contains a significant contribution from the counterions. On the other hand, for the TAA salts in D$_2$O, the SANS contrast is dominated by the counterions, such that $I(q) \propto S_{c,c}(q)$. The SAXS contrast for the TAA salts in H$_2$O, however, arises primarily from the polymer backbone (eqn (2)), with the exception of TBACMC, for which the backbone and counterion contribute similarly to $S(q)$. The contrast conditions are summarised in Table 2.

B. Influence of counterion on scattering properties of CMC

1. High-q scattering: local conformation. SANS profiles for the alkaline salts of CMC in D$_2$O were fitted to eqn (8). This required three fitting parameters: the background term I_{Bck} (which contains contributions from spin and compositional incoherent scattering), the chain cross-sectional radius R_C and the pre-factor A, which is a function of polymer concentration and contrast. Following earlier work,[42] we set $R_C = 3.5$ Å for all fits. The background term and the concentration are left as fitting parameters. The fitted concentration (c_{fit}) is found to be $\simeq 0.7 \times c_g$, where c_g is the concentration calculated from the weights of the polymer and solvent used to prepare the solution. A part of the discrepancy between these two quantities may be taken to indicate a small amount of residual water in the polymer which is not removed by the freeze-drying process. This is confirmed by TGA experiments, which show a mass loss of $\approx 5\%$ for the tetrabutyl-ammonium carboxymethyl cellulose (TBACMC) powder when heated to 120 °C under nitrogen, see Fig. S1 (ESI†). Further errors

presumably arise due to uncertainties in the calculation of the scattering contrast. TGA experiments reveal a consistent mass loss of 5% to 10% upon heating to 120 °C for all the CMC salts studied, and in the following, we assume that to be the water content for all the freeze-dried polymers.

2. Mid-q: the polyelectrolyte peak region. Fig. 2 shows the background subtracted SANS intensities for CMC with alkali counterions at $c = 0.05$ mol L^{-1} and $c = 0.15$ mol L^{-1} in D$_2$O solution. The procedure for subtracting the background term follows our earlier discussion. The curves display a correlation peak at $q = q^\star$ and the value of $q^\star$ is determined by fitting a polynomial to the curves (see Fig. S4 in the ESI†). The peak position ($q^\star$) is found to remain invariant when the counterions are changed as demonstrated by the determined values (indicated by the vertical lines). The total (unnormalized) scattering intensity is seen to depend on the counterion type. These differences are primarily the result of the different scattering length densities of the ions. If the scattering intensity is normalised by the effective contrast (eqn (6)), the resulting
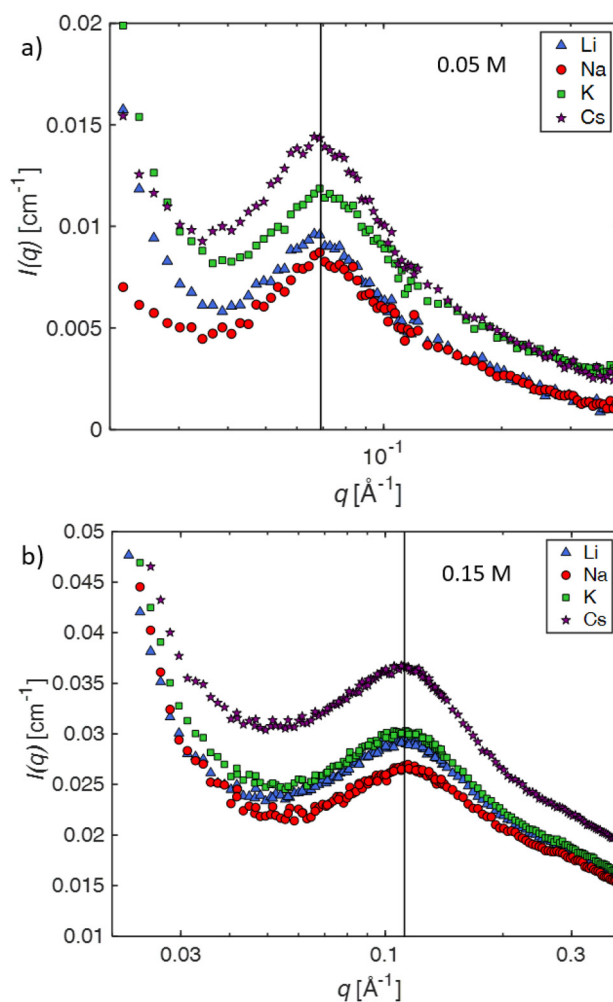
Fig. 2 Background subtracted SANS scattering intensity as a function of scattering wavevector q for alkaline salts of CMC in salt-free D$_2$O, see legend for the colour scheme. a: $c = 0.05$ mol L^{-1} and b: 0.15 mol L^{-1}. Lines indicate the peak positions (a: $q^\star = 0.069$ Å^{-1}, b: $q^\star = 0.112$ Å^{-1}).
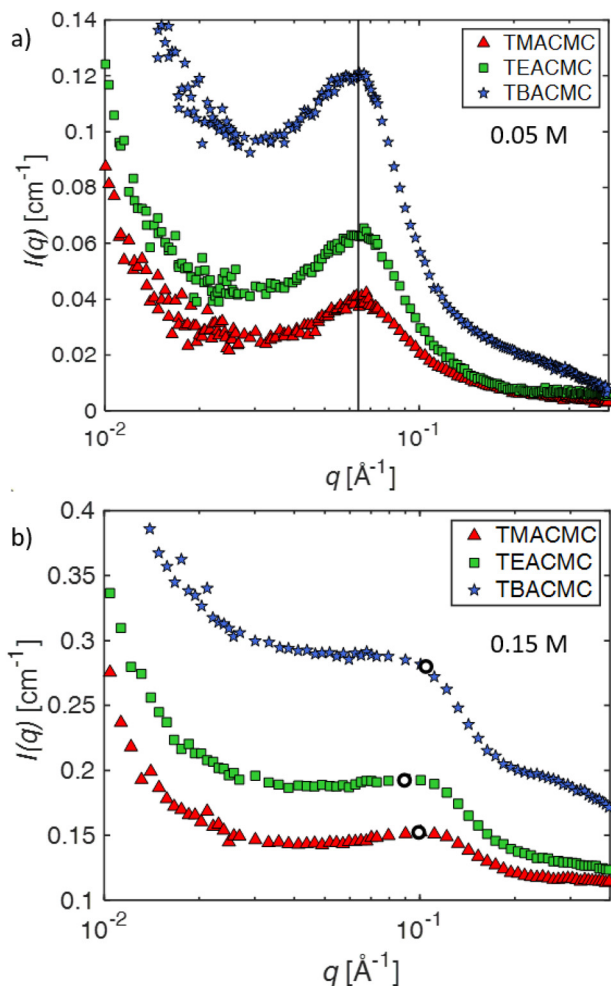
Fig. 3 SANS scattering intensity I as a function of scattering wavevector q for tetra-alkylammonium salts of CMC, see legend for colour scheme. a: $c = 0.05$ mol L^{-1} and b: 0.15 mol L^{-1}. The line indicates the position of the peaks at that concentration ($q^* = 0.064$ Å^{-1}). The hollow points represent the peak positions in TMACMC and TEACMC and the scattering plateau position in TBACMC.

Table 3 B-Coefficients for different ions. Values are from ref. 104

Ion	Jones–Dole B coefficient [L mol^{-1}]
Li$^+$	0.146
Na$^+$	0.085
K$^+$	−0.009
Cs$^+$	−0.047
TMA$^+$	0.123
TEA$^+$	0.385
TBA$^+$	1.275

than $\approx 20\%$. For reference, the viscosity B-coefficients of tetraalkylammonium ions, characterizing their relative strength of the hydration[102,103] are listed in Table 3. These complex ions are strongly "kosmotropic" (i.e. have large positive B-coefficient values) according to the conventional nomenclature, but this designation must be made with caution for large counter-ions since large positive concentration virial coefficients for the viscosity, i.e., the "intrinsic viscosity", are characteristic of polymer solutions. The TAA counter-ion molecules have an alkane polymer component that probably does not hydrate very well so that a large contribution to the viscosity B-coefficient probably derives from a hydrodynamic effect rather than from the strength of the ion–water interaction as in the case of alkaline and other elemental ions.[27]

The concentration dependence of the correlation length for the alkaline salts of CMC agrees well with the scaling prediction (eqn (1)), as expected based on previous SANS and SAXS studies on aqueous solutions of NaCMC.[50,51,64] Applying eqn (1) and (9), the stretch parameter is estimated to be in the range of $B_s \simeq 1.3 \pm 0.1$ for all samples, see Table 4. These values are similar to the stretch parameter of $B_s \simeq 1.1 \pm 0.1$ reported by Lopez et al.[50] for solutions of NaCMC with DS $\simeq 1.06$ in D$_2$O and $B_s \simeq 1.25$ and reported by Hou et al.[105] for NaCMC with DS $\simeq 0.98$ in H$_2$O.

The independence of the peak position on counterion type for the alkaline series contrasts with results for aqueous solutions of ionenes, where the scaling of the peak position with concentration of halide salts of the same polymer depends on the counterion.[80,106,107] Note that Kaji et al. report a weak dependence of the peak position on counterion type for the alkaline salts of poly(vinyl hydrogen sulfate).[108] These results are apparently in line with the simulations observations of Chremos and co-workers discussed previously indicating that stronger ion and polymer solvation, acting together, can alter the concentration scaling of q^*.

The tetra-alkyl-ammonium salts of CMC display similar behaviour to the alkaline salts at low concentrations: the

apparent structure factors $S(q)$ largely overlap, with some of the difference arising from uncertainties in the calculation of the contrasts, as shown in the ESI† (Fig. S2).

The SANS profiles of CMC with tetra-alkyl-ammonium counterions, where the alkyl chain = C1, C2 and C4 in D$_2$O solutions are plotted in Fig. 3. At $c = 0.05$ mol L^{-1}, there is no discernible influence of counterion type on the position of the peak position q^* (Fig. 3(a)). At high concentrations, however, the correlation peak broadens and moves to a lower q for the larger counterions. For sufficiently high concentrations ($c \simeq 0.15$ mol L^{-1}), the peak in TBACMC solutions develops into a scattering plateau (i.e. no discernible maxima) where a polynomial fit is no longer possible. Here, we fit two linear functions to either side of the scattering plateau, following the approach of Salamon et al.,[73] and take their point of the intersection to be the 'position' of the scattering plateau (see Fig. S4 in the ESI†). If this method is applied for samples with a distinct peak, the difference in q^* compared to the value extracted from fitting a polynomial is always smaller

Table 4 B_s – parameter estimated from SANS and SAXS measurements using eqn (1) over the concentration ranges indicated

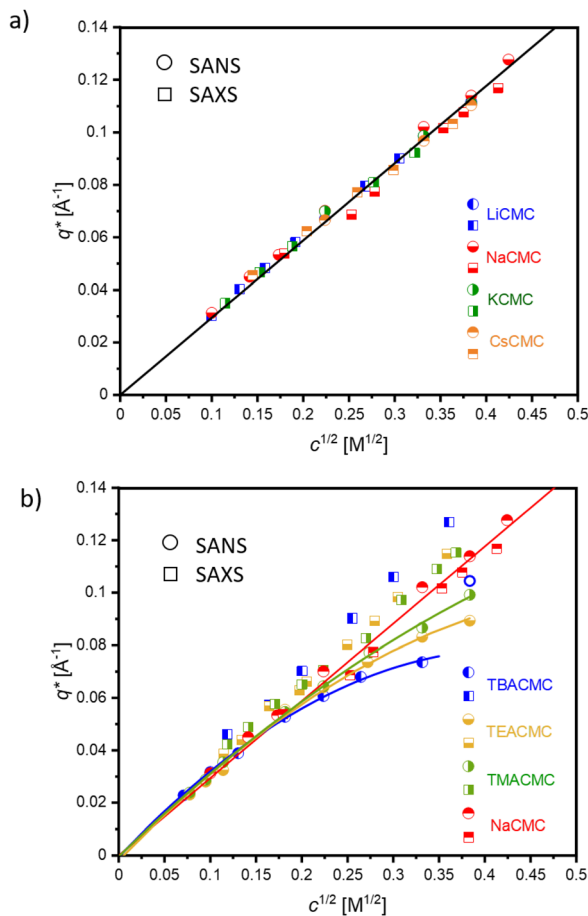| CMC salt	$B_{s,SANS}$	c-range [M]	$B_{s,SAXS}$	c-range [M]
LiCMC	1.4	0.05–0.147	1.24	0.009–0.087
NaCMC	1.2	0.01–0.18	1.40	0.033–0.15
KCMC	1.36	0.05– 0.147	1.27	0.012–0.096
CsCMC	1.43	0.05–0.147	1.31	0.021–0.132
TMACMC	1.22	0006–0.033	1.08	0.013–0.126
TEACMC	1.32	0.006–0.05	1.07	0.012–0.119
TBACMC	1.18	0.003–0.017	0.92	0.025–0.121

a)

b)

Fig. 4 Peak positions (q^*) as determined from SANS (circles) and SAXS (squares) curves for CMCs with (a) alkaline and (b) tetra-alkyl-ammonium counterions in water as a function of concentration, see legend for the colour scheme. Hollow symbols are for the fit scattering plateaus.

correlation length is independent of ion type, matching the values observed for alkaline CMCs (see Fig. 4(b)), the maxima in $S_{mm}(q)$ and $S_{cc}(q)$ coincide and the common scaling $q^* \sim c^{1/2}$ is observed. These observations accord with literature reports for polystyrene sulfonate (PSS). Prabhu *et al.* report the correlation lengths for TMAPSS in D_2O ($3.7 < c < 46$ g L^{-1}), measured by SANS,[109] which are nearly identical values to those reported for NaPSS in H_2O obtained using SANS and SAXS.[78,110–113]

At high concentrations, however, the behaviour of TAA salts differs in several ways from those of alkaline salts. First, the peak position in the SANS signal, which measures $S_{cc}(q)$, shifts to lower q values and its shape becomes broader, eventually morphing into a scattering "plateau". The magnitude of these changes depends on the length of the alkyl chain, with larger ions showing more pronounced effects, see for example Fig. 4b. The maxima in the SAXS signal, which corresponds approximately to $S_{mm}(q)$ is almost the same as for the alkaline counterions. These results indicate that (1) polymer correlation scale (inferred from q^*) is not greatly altered by the nature of the counterions and (2) the concentration fluctuations of the polymer backbone and the counterions become decoupled at high concentrations if the counterions are strongly kosmotropic, *i.e.*,

relatively large positive values of B, see Table 3. For a discussion on the decoupling of polymer and charge concentration fluctuations, see also ref. 114 and 115.

The partial molar volume of the TBA^+ ion can be used to calculate an ionic radius of $\simeq 0.5$ nm, in agreement with the radius expected from bond lengths. At the highest concentrations studied, this corresponds to the bare ions occupying a volume fraction of $\simeq 0.05$. If a hydration volume corresponding to 20–40 water molecules per ion is added,[116] the volume fraction of the hydrated TAA ions increases to 0.1–0.15. This might be sufficient for the hydrated ions to percolate, which we anticipate influences the average intermolecular potential between the polyelectrolytes deriving from the competitive association of hydrated counter-ions and water molecules with the polyelectrolyte chains. In particular, we expect the extended counter-ion cloud found for low-concentration polyelectrolyte solutions to become delocalized when the counter-ion concentration becomes sufficiently large that their hydration layers percolate, suppressing the large-scale fluctuations in the concentration of the counter-ions about the polyelectrolyte chains responsible for the long-range attractive interactions between polymers having a like charge sign. However, this proposed mechanism of the polyelectrolyte peak suppression remains to be checked by molecular dynamics simulation and we simply offer this as a tentative hypothesis.

An important implication of this hypothesis for the progressive suppression of the polyelectrolyte peak at high salt concentrations seems to be supported by our measurements is that percolation concentration or "overlap concentration" of the counter-ion molecules should govern the concentration at which this transition in polyelectrolyte solution should occur. As in the case of neutral polymer solutions, the concentration corresponding to the TAA counterion overlap becomes smaller when their molecular mass becomes larger. We note that the suppression of the polyelectrolyte peak at high salt concentrations is a well-known trend in polyelectrolyte solutions,[117] although it is by no means established that this trend is simply due to charge screening in the simple Debye–Huckel sense. Here, we are simply suggesting that the percolation of the hydrated counterions is influencing the strength of the many-body intermolecular interaction strength between the polyelectrolytes.

3. The low-q upturn: large scale inhomogeneities. Fig. 5(a) plots the scattering intensity of carboxymethyl cellulose with four different counterions at a concentration of $c = 0.11$ mol L^{-1}. The low-q upturn can be fitted to a power-law in the low-q region (eqn (10)), although it is unclear if the data follow a single power-law over a wide q-range. The best-fit exponent is plotted as a function of concentration in Fig. 5(b). The exponent for the TMA and TEA salts shows a decrease with concentration, and for $c \geq 0.11$ mol L^{-1} it converges with the value $m \approx 3.6$ observed for TBACMC over the entire concentration range, indicated by the dashed line. The same value was reported by Lopez *et al.* for NaCMC in D_2O in an earlier study.[42] The large value of the exponents suggests that the entities responsible for the upturn are surface fractals or have diffuse interfaces.
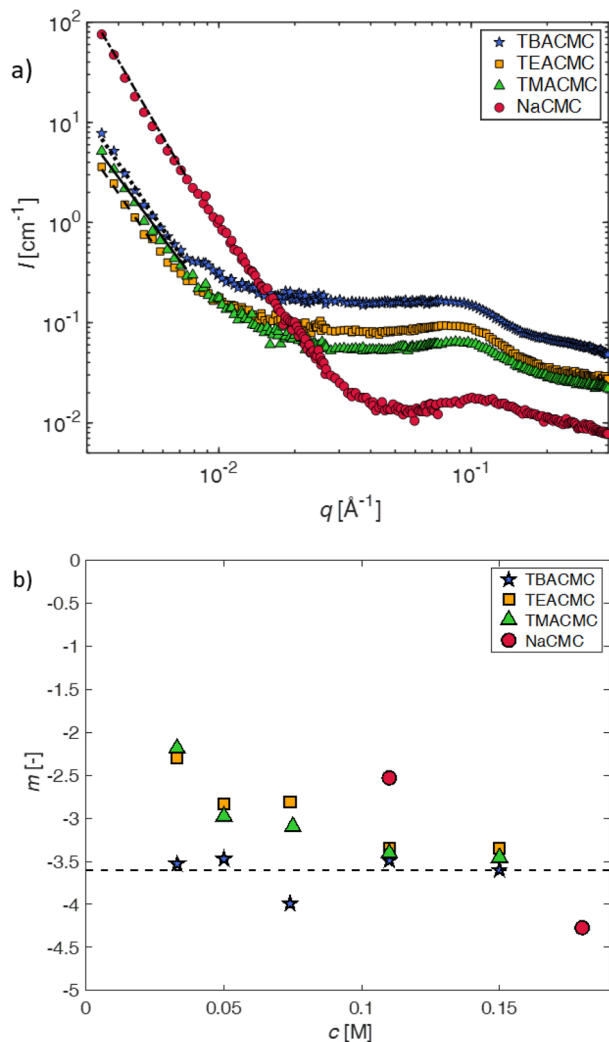
Fig. 5 (a) SANS scattering intensity of CMC with different counterions for a fixed concentration of c = 0.11 mol L^{-1}. Lines are power-law fits (eqn (10)) to the low-q upturn region. (b) Best-fit exponent $-m$ as a function of polymer concentration for various salts of CMC.

Fig. 6 (a) Pre-factor to clustering power-law (D), normalised by effective SANS scattering contrast ($\bar{b}_{eff}$) as a function of counterion type. The parameter $D/\bar{b}_{eff}$ serves as a measure of clustering strength. (b) Scattering intensity at q = 0.0034 Å^{-1} normalised by effective contrast. Data for carbon chain length = 0 are for NaCMC.

The pre-factor, D, to the low-q power-law in eqn (10) is plotted as a function of ion type in Fig. 6(a) for c = 0.11 mol L^{-1} and c = 0.15 mol L^{-1}. For this plot, we use fits with the exponent m fixed to a value of 3.6, so that the units of the pre-factor are independent of concentration. We have divided D by $\bar{b}_{eff}$ to reduce the influence of neutron contrast. Further, we compare the scattering intensity at the lowest measured wave vector (q = 0.0034 Å^{-1}) at c = 0.11 mol L^{-1} for the various salts studied. Lacking a more rigorous framework to evaluate the low-q region, both $D/\bar{b}_{eff}$ and I(0.0034 Å^{-1})$/\bar{b}_{eff}$ serve as measures for the 'clustering strength'.[118–121] The trends observed in Fig. 6 therefore support an earlier finding by molecular dynamics simulations[29] that preferential counterion solvation can lead to enhanced clustering in polyelectrolyte solutions. The general increase of the clustering strength parallels the growth of the viscosity B-coefficient values[122] of the tetra-alkylammonium counterions.
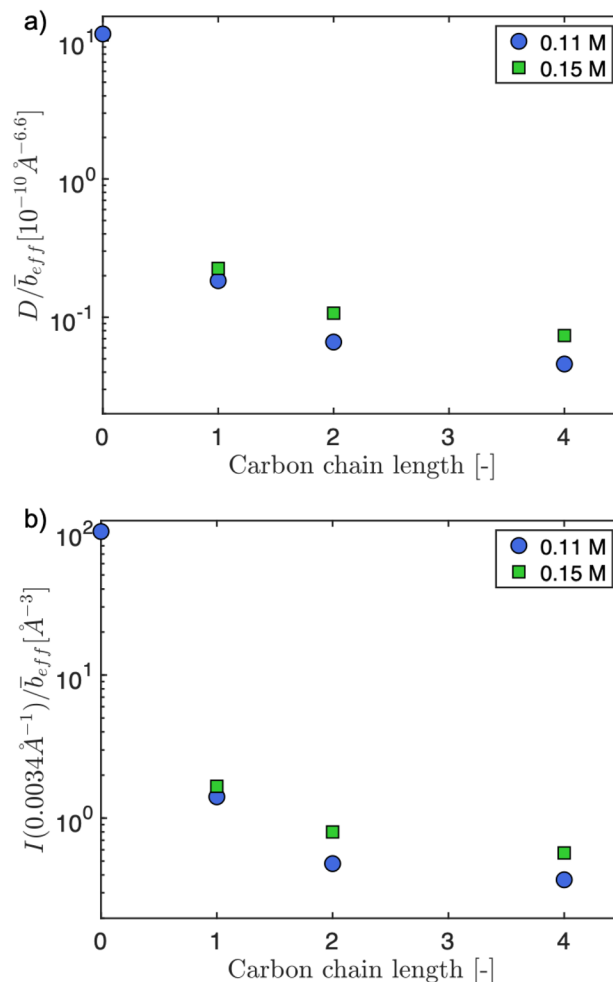
V. Conclusions

We have studied the scattering properties of semiflexible poly-electrolyte carboxymethyl cellulose with different counterions in aqueous solutions. The correlation peak of the various alkaline salts studied follows the same $q^* \propto c^{1/2}$ scaling law and the peak positions measured by SANS and SAXS agree, indicating that concentration fluctuations of the polymer backbone and counterions occur on approximately the same lengthscales.

Solutions with hydrophobic counterions display similar features to the alkaline salts at low concentrations. However, beyond a characteristic concentration, a different scaling behaviour emerges. First, in this regime, the c-dependence of q^*, obtained from SANS, becomes increasingly weaker with an increasing degree of counterion hydrophobicity. However, the $q^* \propto c^{1/2}$ scaling persists in the results obtained from SAXS, even for the most hydrophobic counterion studied. We interpret this as a "decoupling" of the concentration fluctuations of

the polymer backbone and counterions, but we, currently, lack any convincing explanation for the physical mechanism underpinning this behaviour. A further examination of the nature of counterion-solvent interactions using other techniques, such as rheology, could provide better insights into this behaviour. In this regard, a recent study of polystyrene sulfonate with sodium and tetra-alkyl ammonium counterions showed that the viscosity of PSS salts is independent of counterion type at low ($c \lesssim 0.1$ M) concentrations, but differs strongly at high concentrations.[12] Another key observation at higher concentrations is the broadening of the SANS correlation peaks with increasing counterion hydrophobicity. This is accompanied by a shift in the correlation peak position as well.

As with other polyelectrolyte systems, the solutions studied here displayed an upturn at low q, which signals the presence of large-scale inhomogeneities in the solution. A comparison of solutions of sodium and tetra-alkyl-ammonium salts of CMC revealed that the clustering intensity, when adjusted for contrast, decreases as the ions become larger and more hydrophobic. The nature of hydration in these complex ions requires further investigation.

Author contributions

CRediT: Anish Gulati: formal analysis, investigation, data curation, methodology, writing – original draft, writing – review & editing. Jack F. Douglas: formal analysis, investigation, writing – original draft, writing – review & editing. Olga Matsarskaia: data curation, investigation, methodology, writing – review & editing Carlos G. Lopez: conceptualization, formal analysis, funding acquisition, investigation, data curation, methodology, supervision, writing – original draft, writing – review & editing.

Data availability

All the scattering datasets from this study are included in xls format as ESI.†

Conflicts of interest

There are no conflicts to declare.

Acknowledgements

References

1 A. V. Dobrynin and M. Rubinstein, *Prog. Polym. Sci.*, 2005, **30**, 1049–1118.

2 R. H. Colby, *Rheol. Acta*, 2010, **49**, 425–442.

3 C. G. Lopez, A. Matsumoto and A. Q. Shen, *Soft Matter*, 2024, **20**, 2635–2687.

4 C. G. Lopez, F. Horkay, M. Mussel, R. L. Jones and W. Richtering, *Soft Matter*, 2020, **16**, 7289–7298.

5 Y. Zhang, J. F. Douglas, B. D. Ermi and E. J. Amis, *J. Chem. Phys.*, 2001, **114**, 3299–3313.

6 E. Dubois and F. Boué, *Macromolecules*, 2001, **34**, 3684–3697.

7 J.-S. Jan and V. Breedveld, *Macromolecules*, 2008, **41**, 6517–6522.

8 I. Kagawa and R. M. Fuoss, *J. Polym. Sci.*, 1955, **18**, 535–542.

9 M. Beer, M. Schmidt and M. Muthukumar, *Macromolecules*, 1997, **30**, 8375–8385.

10 R. Schweins, J. Hollmann and K. Huber, *Polymer*, 2003, **44**, 7131–7141.

11 A. Gulati, M. Jacobs, C. G. Lopez and A. V. Dobrynin, *Macromolecules*, 2023, **56**, 2183–2193.

12 A. Gulati and C. G. Lopez, *ACS Macro Lett.*, 2024, **13**, 1079–1083.

13 A. Matsumoto and A. Q. Shen, *Soft Matter*, 2022, **18**, 4197–4204.

14 E. Seyrek and P. Dubin, *Adv. Colloid Interface Sci.*, 2010, **158**, 119–129.

15 A. Katchalsky, *Biophys. J.*, 1964, **4**, 9–41.

16 M. Rubinstein and G. A. Papoian, *Soft Matter*, 2012, **8**, 9265–9267.

17 A. V. Dobrynin, R. H. Colby and M. Rubinstein, *Macromolecules*, 1995, **28**, 1859–1871.

18 P. Pfeuty, *J. Phys. Colloq.*, 1978, **39**, C2-149.

19 P. D. Gennes, P. Pincus, R. Velasco and F. Brochard, *J. Phys.*, 1976, **37**, 1461–1473.

20 M. Yamaguchi, M. Wakutsu, Y. Takahashi and I. Noda, *Macromolecules*, 1992, **25**, 470–474.

21 A. V. Dobrynin and M. Rubinstein, *Prog. Polym. Sci.*, 2005, **30**, 1049–1118.

22 A. V. Dobrynin and M. Jacobs, *Macromolecules*, 2021, **4**, 1859–1869.

23 A. Chremos and J. F. Douglas, *J. Chem. Phys.*, 2017, **147**, 241103.

24 A. Chremos and F. Horkay, *Phys. Rev. E*, 2020, **102**, 012611.

25 A. Chremos and J. F. Douglas, *J. Chem. Phys.*, 2018, **149**, 163305.

26 C. Hotton, G. Ducouret, J. Sirieix-Plénet, T. Bizien, L. Porcar and N. Malikova, *Macromolecules*, 2023, **56**, 923–933.

27 J. A. Clark and J. F. Douglas, *J. Phys. Chem. B*, 2024, **128**, 6362–6375.

28 A. Chremos and J. F. Douglas, *Gels*, 2018, **4**, 20.

29 A. Chremos and J. F. Douglas, *J. Chem. Phys.*, 2018, **149**, 163305-1–163305-11.

30 F. Horkay, A. Chremos, J. F. Douglas, R. Jones, J. Lou and Y. Xia, *J. Chem. Phys.*, 2021, **155**, 074901-1–074901-13.

31 S. Wang, R. Walker-Gibbons, B. Watkins, M. Flynn and M. Krishnan, *Nat. Nanotechnol.*, 2024, 1–9.

32 A. Behjatian, R. Walker-Gibbons, A. A. Schekochihin and M. Krishnan, *Langmuir*, 2022, **38**, 786–800.

33 M. Sedlák and E. J. Amis, *J. Chem. Phys.*, 1992, **96**, 826–834.

34 M. Sedlak, *J. Chem. Phys.*, 1996, **105**, 10123–10133.

35 M. Sedlák, *Langmuir*, 1999, **15**, 4045–4051.

36 M. Sedlák, *J. Chem. Phys.*, 2002, **116**, 5236–5245.

37 M. Sedlák, *J. Chem. Phys.*, 2002, **116**, 5246–5255.

38 B. D. Ermi and E. J. Amis, *Macromolecules*, 1998, **31**, 7378–7384.

39 S. Ghosh, R. M. Peitzsch and W. F. Reed, *Biopolymers*, 1992, **32**, 1105–1122.

40 M. Sedlak, *Macromolecules*, 1993, **26**, 1158–1162.

41 C. Kosgallana, M. Senanayake, S. S. Mohottalalage, S. Wijesinghe, L. He, G. S. Grest and D. Perahia, *Macromolecules*, 2024, 1688–1698.

42 C. G. Lopez, S. E. Rogers, R. H. Colby, P. Graham and J. T. Cabral, *J. Polym. Sci., Part B: Polym. Phys.*, 2015, **53**, 492–501.

43 C. Clasen and W.-M. Kulicke, *Prog. Polym. Sci.*, 2001, **26**, 1839–1919.

44 T. Garlick and P. Miner, *US Pat.*, 3597416, 1993.

45 J. N. Bemiller and R. L. Whistler, *Industrial gums: polysaccharides and their derivatives*, Academic Press, 1992.

46 J. K. Fink, *Water-based chemicals and technology for drilling, completion, and workover fluids*, Gulf Professional Publishing (Elsevier), 2015.

47 F. B. Insights, Market Research Report, 2021.

48 H. Chen, *Lignocellulose biorefinery engineering*, Elsevier, 2015.

49 J. S. Behra, J. Mattsson, O. J. Cayre, E. S. J. Robles, H. Tang and T. N. Hunter, *ACS Appl. Polym. Mater.*, 2019, **1**, 344–358.

50 C. G. Lopez, S. E. Rogers, R. H. Colby, P. Graham and J. T. Cabral, *J. Polym. Sci., Part B: Polym. Phys.*, 2014, **53**, 492–501.

51 C. G. Lopez, R. H. Colby and J. T. Cabral, *Macromolecules*, 2018, **51**, 3165–3175.

52 C. G. Lopez, *J. Rheol.*, 2020, **64**, 191–204.

53 C. Barba, D. Montané, M. Rinaudo and X. Farriol, *Cellulose*, 2002, **9**, 319–326.

54 C. Barba, D. Montané, X. Farriol, J. Desbrières and M. Rinaudo, *Cellulose*, 2002, **9**, 327–335.

55 P. Wagner, S. Różańska, E. Warmbier, A. Frankiewicz and J. Różański, *Materials*, 2023, **16**, 418.

56 L. N. Jimenez, C. D. Martnez Narváez and V. Sharma, *Phys. Fluids*, 2020, **32**, 012113.

57 L. N. Jimenez, C. D. Martinez Narvaez and V. Sharma, *Macromolecules*, 2022, 8117–8132.

58 D. Truzzolillo, F. Bordi, C. Cametti and S. Sennato, *Phys. Rev. E: Stat., Nonlinear, Soft Matter Phys.*, 2009, **79**, 011804.

59 D. Ray, R. De and B. Das, *J. Chem. Thermodyn.*, 2016, **101**, 227–235.

60 E. deButts, J. A. Hudy and J. Elliott, *Ind. Eng. Chem.*, 1957, **49**, 94–98.

61 L. Xiqua, Q. Tingzhu and Q. Shaoqui, *Acta Polym.*, 1990, **41**, 220–222.

62 G. Dürig and A. Banderet, *Helv. Chim. Acta*, 1950, **33**, 1106–1118.

63 J. Enebro, D. Momcilovic, M. Siika-Aho and S. Karlsson, *Biomacromolecules*, 2007, **8**, 3253–3257.

64 W. N. Sharratt, R. O'Connell, S. E. Rogers, C. G. Lopez and J. T. Cabral, *Macromolecules*, 2020, **53**, 1451–1463.

65 C. Castelain, J. Doublier and J. Lefebvre, *Carbohydr. Polym.*, 1987, **7**, 1–16.

66 C. G. Lopez, L. Voleske and W. Richtering, *Carbohydr. Polym.*, 2020, **234**, 115886.

67 H. Vink, *Macromol. Chem. Phys.*, 1982, **183**, 2273–2283.

68 H. Vink, *J. Chem. Soc., Faraday Trans. 1*, 1989, **85**, 699–709.

69 S. Dou and R. H. Colby, *Macromolecules*, 2008, **17**, 6505–6510.

70 J. Combet, M. Rawiso, C. Rochas, S. Hoffmann and F. Boué, *Macromolecules*, 2011, **44**, 3039–3052.

71 P. Lorchat, I. Konko, J. Combet, J. Jestin, A. Johner, A. Laschewski, S. Obukhov and M. Rawiso, *Europhys. Lett.*, 2014, **106**, 28003.

72 C. G. Lopez, F. Horkay, R. Schweins and W. Richtering, *Macromolecules*, 2021, **54**, 10583–10593.

73 K. Salamon, D. Aumiler, G. Pabst and T. Vuletic, *Macromolecules*, 2013, **46**, 1107–1118.

74 L. Wang and V. A. Bloomfield, *Macromolecules*, 1991, **24**, 5791–5795.

75 C. G. Lopez and W. Richtering, *J. Chem. Phys.*, 2018, **148**, 244902.

76 T. Waigh, A. Papagiannopoulos, A. Voice, R. Bansil, A. Unwin, C. Dewhurst, B. Turner and N. Afdhal, *Langmuir*, 2002, **18**, 7188–7195.

77 W. F. Reed, *J. Chem. Phys.*, 1994, **100**, 7825–7827.

78 K. Kaji, H. Urakawa, T. Kanaya and R. Kitamaru, *J. Phys.*, 1988, **49**, 993–1000.

79 K. Nishida, K. Kaji and T. Kanaya, *J. Chem. Phys.*, 2001, **115**, 8217–8220.

80 N. Malikova, A.-L. Rollet, S. Čebašek, M. Tomšič and V. Vlachy, *Phys. Chem. Chem. Phys.*, 2015, **17**, 5650–5658.

81 A. Chremos and J. F. Douglas, *J. Chem. Phys.*, 2017, **147**, 044906.

82 F. Boué, J. Combet, B. Demé, M. Heinrich, J.-G. Zilliox and M. Rawiso, *Polymers*, 2016, **8**, 228.

83 G. Nisato, R. Ivkov and E. J. Amis, *Macromolecules*, 1999, **32**, 5895–5900.

84 A. Ramzi, R. Scherrenberg, J. Joosten, P. Lemstra and K. Mortensen, *Macromolecules*, 2002, **35**, 827–833.

85 H. Inoue and T. Matsumoto, *J. Rheol.*, 1994, **38**, 973–984.

86 D. Renard, M. A. Axelos, F. Boué and J. Lefebvre, *Biopolymers*, 1996, **39**, 149–159.

87 F. Muller, M. Delsanti, L. Auvray, J. Yang, Y. Chen, J. Mays, B. Demé, M. Tirrell and P. Guenoun, *Eur. Phys. J. E: Soft Matter Biol. Phys.*, 2000, **3**, 45–53.

88 P. Guenoun, M. Delsanti, D. Gazeau, J. Mays, D. Cook, M. Tirrell, M. Tirrell and L. Auvray, *Eur. Phys. J. B*, 1998, **1**, 77–86.

89 K. Kassapidou, W. Jesse, M. Kuil, A. Lapp, S. Egelhaaf and J. Van der Maarel, *Macromolecules*, 1997, **30**, 2671–2684.

90 K. Nishida, K. Kaji, T. Kanaya and T. Shibano, *Macromolecules*, 2002, **35**, 4084–4089.

91 We neglect here the scattering from the counterions, which is a valid approximating under certain conditions, as discussed later in the manuscript.

92 L. Schulz, B. Seger and W. Burchard, *Macromol. Chem. Phys.*, 2000, **201**, 2008–2022.

93 P. W. Schmidt, *The fractal approach to heterogeneous chemistry*, 1989, pp. 67–79.

94 F. Cousin, J. Gummel, D. Ung and F. Boué, *Langmuir*, 2005, **21**, 9675–9688.

95 P. Vallat, J.-M. Catala, M. Rawiso and F. Schosseler, *Macromolecules*, 2007, **40**, 3779–3783.

96 C. G. Lopez and W. Richtering, *Cellulose*, 2019, **26**, 1517–1534.

97 S. Pyett and W. Richtering, *J. Chem. Phys.*, 2005, **122**, 034709.

98 Certain commercial equipment, instruments, or materials are identified in this paper to foster understanding. Such identification does not imply recommendation or endorsement by the National Institute of Standards and Technology, nor does it imply that the materials or equipment identified are necessarily the best available for the purpose.

99 C. Wandrey, A. Bartkowiak and D. Hunkeler, *Langmuir*, 1999, **15**, 4062–4068.

100 Y. Marcus, *J. Phys. Chem. B*, 2009, **113**, 10285–10291.

101 L. H. Blanco and E. F. Vargas, *J. Solution Chem.*, 2006, **35**, 21–28.

102 M. Andreev, A. Chremos, J. de Pablo and J. F. Douglas, *J. Phys. Chem. B*, 2017, **121**, 8195–8202.

103 M. Andreev, J. J. de Pablo, A. Chremos and J. F. Douglas, *J. Phys. Chem. B*, 2018, **122**, 4029–4034.

104 H. D. B. Jenkins and Y. Marcus, *Chem. Rev.*, 1995, **95**, 2695–2724.

105 C. Hou, T. Watanabe, C. G. Lopez and W. Richtering, *Carbohydr. Polym.*, 2025, **347**, 122287.

106 N. Malikova, S. Čebašek, V. Glenisson, D. Bhowmik, G. Carrot and V. Vlachy, *Phys. Chem. Chem. Phys.*, 2012, **14**, 12898–12904.

107 C. Hotton, Y. Sakhawoth, A.-L. Rollet, J. Sireix-Plénet, L. Tea, S. Combet, M. Sharp, I. Hoffmann, F. Nallet and N. Malikova, *C. R. Chim.*, 2024, DOI: **10.26434/chemrxiv-2024-drcrc**.

108 K. Kaji, H. Urakawa, T. Kanaya and R. Kitamaru, *Macromolecules*, 1984, **17**, 1835–1839.

109 V. M. Prabhu, E. J. Amis, D. P. Bossev and N. Rosov, *J. Chem. Phys.*, 2004, **121**, 4424–4429.

110 V. Prabhu, M. Muthukumar, G. D. Wignall and Y. B. Melnichenko, *J. Chem. Phys.*, 2003, **119**, 4085–4098.

111 J. Combet, F. Isel, M. Rawiso and F. Boué, *Macromolecules*, 2005, **38**, 7456–7469.

112 K. Nishida, K. Kaji and T. Kanaya, *J. Chem. Phys.*, 2001, **114**, 8671–8677.

113 M. Nierlich, F. Boue, A. Lapp and R. Oberthür, *Colloid Polym. Sci.*, 1985, **263**, 955–964.

114 M. Jacobs, C. G. Lopez and A. V. Dobrynin, *Macromolecules*, 2021, **54**, 9577–9586.

115 A. V. Dobrynin and M. Jacobs, *Macromolecules*, 2021, **54**, 1859–1869.

116 Y. Marcus, *J. Solution Chem.*, 2008, **37**, 1071–1098.

117 B. D. Ermi and E. J. Amis, *Macromolecules*, 1997, **30**, 6937–6942.

118 B. Hammouda, F. Horkay and M. L. Becker, *Macromolecules*, 2005, **38**, 2019–2021.

119 B. Hammouda, *Polymer*, 2009, **50**, 5293–5297.

120 F. Horkay and B. Hammouda, *Colloid Polym. Sci.*, 2008, **286**, 611–620.

121 B. Hammouda, *J. Chem. Phys.*, 2010, **133**(8), 084901.

122 R. L. Kay, T. Vituccio, C. Zawoyski and D. Evans, *J. Phys. Chem. B*, 1966, **70**, 2336–2341.